
PHASE COLLAPSE IN NEURAL NETWORKS

Florentin Guth, John Zarka

Département d'informatique de l'ENS, ENS, CNRS, PSL University, Paris, France
 {florentin.guth, john.zarka}@ens.fr

Stéphane Mallat

Collège de France, Paris, France
 Flatiron Institute, New York, USA

ABSTRACT

Deep convolutional image classifiers progressively transform the spatial variability into a smaller number of channels, which linearly separates all classes. A fundamental challenge is to understand the role of rectifiers together with convolutional filters in this transformation. Rectifiers with biases are often interpreted as thresholding operators which improve sparsity and discrimination. This paper demonstrates that it is a different phase collapse mechanism which explains the ability to progressively eliminate spatial variability, while improving linear class separation. This is explained and shown numerically by defining a simplified complex-valued convolutional network architecture. It implements spatial convolutions with wavelet filters and uses a complex modulus to collapse phase variables. This phase collapse network reaches the classification accuracy of ResNets of similar depths, whereas its performance is considerably degraded when replacing the phase collapse with thresholding operators. This is justified by explaining how iterated phase collapses progressively improve separation of class means, as opposed to thresholding non-linearities.

1 INTRODUCTION

CNN image classifiers progressively eliminate spatial variables through iterated filterings and subsamplings, while linear classification accuracy improves as depth increases (Oyallon, 2017). It has also been observed numerically that CNNs concentrate training samples of each class in small separated regions of a progressively lower-dimensional space. It can ultimately produce a “neural collapse” (Papayan et al., 2020), where all training samples of each class are mapped to a single point. In this case, the elimination of spatial variables comes with a collapse of within-class variability and perfect linear separability. Increases in linear classification accuracy are obtained by iterating linear convolutional operators and ReLUs with biases. A difficulty in understanding the underlying mathematics comes from the flexibility of ReLUs. Any non-linearity can indeed be approximated by a linear combination of biased ReLUs. Many papers interpret iterations on ReLUs and linear operators as sparse code computations (Sun et al., 2018; Sulam et al., 2018; 2019; Mahdizadehaghdam et al., 2019; Zarka et al., 2020; 2021). We show that these classification improvements by eliminating spatial variabilities rather come from a phase collapse, which eliminates the phase of network coefficients. This is demonstrated by introducing a structured convolutional neural network, with wavelet filters and no bias.

Images are defined over a grid whose topology is generated by a translation operator. Translations are diagonalized in the Fourier basis, where they become a complex phase shift. This is why complex-valued representations reveal the mathematics of spatial variability. Invariants are computed with a modulus which collapses all phases. Section 2 explains how this phase collapse can improve linear classification with complex-valued filters. A CNN with complex-valued filters is just a particular instance of a real-valued CNN, whose channels are paired together to define complex numbers. A phase collapse can as well be calculated with ReLUs on real network coefficients.

To demonstrate the role of phase collapse in classifiers, as opposed to thresholding or more general amplitude reduction operators, Section 3 introduces a Phase Collapse Scattering network. It applies a learned 1×1 convolutional complex operator P_j on each layer x_j , followed by a complex wavelet filtering operator W , which outputs coefficients whose phases are eliminated by a modulus:

$$x_{j+1} = |WP_j x_j|. \quad (1)$$

It thus involves no bias. By incorporating a skip-connection, we show that this phase collapse network reaches ResNet accuracy on ImageNet and CIFAR-10. This network architecture is illustrated in Figure 1. We show that replacing the phase collapse modulus by a soft-thresholding or more general amplitude reduction non-linearities considerably decreases the classification accuracy.

Section 4 explains the performance of iterated phase collapses by showing that it progressively improves linear discriminability. On the opposite, iterating soft-thresholdings with optimized linear operators can only marginally improve sparsity and classification.

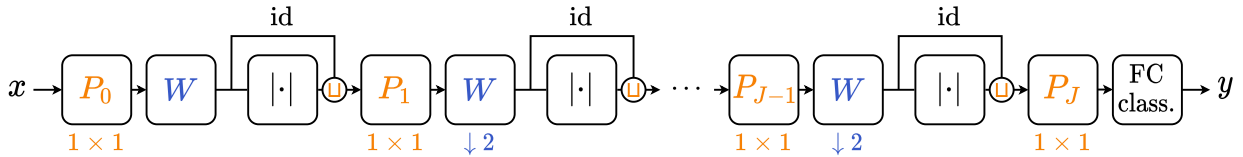


Figure 1: Architecture of a Phase Collapse Scattering network. Orange denotes channel operators while blue denotes spatial operators. The network consists of J elementary computational blocks, with $J = 11$ for ImageNet and $J = 8$ for CIFAR-10. Each block is composed sequentially of: a learned 1×1 convolutional operator P_j , a convolutional wavelet filtering operator W , and a complex modulus $|\cdot|$ which eliminates complex phases. A skip-connection concatenates the outputs of WP_j and $|WP_j|$. A subsampling by 2 is applied after W every other block. A final 1×1 P_J reduces the dimension before a linear classifier.

The main contribution of this paper is a demonstration that the classification accuracy of deep neural networks mostly relies on phase collapses, which are both necessary and sufficient to linearly separate the different class means on complex image databases. This is captured by the Phase Collapse Scattering architecture which reaches ResNet-18 accuracy on ImageNet and CIFAR-10. The code to reproduce the experiments in the paper is available in the supplementary material.

2 PHASE COLLAPSE VERSUS THRESHOLDINGS AND RELUS

A CNN classifier performs a non-linear transformation of an image spatial variability into a smaller number of channels, which linearly separates the different classes. A linear projector can arbitrarily reduce dimensionality, but does not improve linear separability. Linear separability can however be improved by non-linear operators. We show that a phase collapse is necessary to separate classes that are locally invariant to translations. We also analyze the effect of other non-linearities such as soft-thresholdings and ReLUs.

Translations and phase shifts Translations capture the spatial topology of the grid on which the image is defined. Translations are represented by phase shifts in a Fourier transform, and we prove that it remains approximately valid for images convolved with appropriate complex filters.

Let x be an image indexed by $u \in \mathbb{Z}^2$. We write $x_\tau(u) = x(u - \tau)$ the translation of x by τ . It is diagonalized by the Fourier transform $\widehat{x}(\omega) = \sum_u x(u) e^{-iu \cdot \omega}$, which creates a phase shift:

$$\widehat{x}_\tau(\omega) = e^{-i\tau \cdot \omega} \widehat{x}(\omega). \quad (2)$$

This diagonalization explains the need to introduce complex numbers to analyze the mathematical properties of spatial image variabilities, although computations can be carried with real numbers.

A Fourier transform is computed by filtering x with complex exponentials $e^{i\omega \cdot u}$. One may replace these exponentials by localized complex filters ψ . The following theorem proves that small translations can still be approximated by a phase shift in this case.

Theorem 1. *Let $\psi: \mathbb{Z}^2 \rightarrow \mathbb{C}$ be a filter with $\|\psi\|_2 = 1$, whose center frequency ξ and bandwidth σ are defined by:*

$$\xi = \frac{1}{(2\pi)^2} \int_{[-\pi, \pi]^2} \omega |\widehat{\psi}(\omega)|^2 d\omega \text{ and } \sigma^2 = \frac{1}{(2\pi)^2} \int_{[-\pi, \pi]^2} |\omega - \xi|^2 |\widehat{\psi}(\omega)|^2 d\omega.$$

Then, for any $\tau \in \mathbb{Z}^2$,

$$\|x_\tau * \psi - e^{-i\xi \cdot \tau} (x * \psi)\|_\infty \leq \sigma |\tau| \|x\|_2. \quad (3)$$

The proof is in Appendix A. This theorem proves that if $|\tau| \ll 1/\sigma$, then $x_\tau * \psi \approx e^{-i\xi \cdot \tau} x * \psi$. The translation by τ then produces a phase shift of $\xi \cdot \tau$.

Phase collapse and stationarity A phase collapse eliminates the phase of a complex number with a modulus. Over Fourier coefficients, it defines translation-invariant coefficients: $|\widehat{x}_\tau| = |\widehat{x}|$. We show that phase collapses improve linear classification of translation-invariant or locally translation-invariant classes.

Each class indexed by y may be represented by a random vector X_y , whose realizations are the class samples. These classes are linearly separable if their expected values $\mathbb{E}[X_y]$ are all different, and if each $\mathbb{E}[X_y]$ is sufficiently well-estimated by a linear operator applied to a realization x of X_y (Hastie et al., 2009). If the classes are locally or globally invariant to translations, then all X_y are locally or globally stationary.

A stationary process has a probability distribution which is invariant to translations. Equation (2) implies that the phase of its Fourier coefficients has a probability distribution uniformly distributed in $[0, 2\pi]$. If all X_y are stationary, then $\mathbb{E}[\widehat{X}_y(\omega)] = 0$ for $\omega \neq 0$, so these Fourier coefficients do not provide any discriminative information for classification. A phase collapse is then necessary to create non-zero means from these Fourier coefficients. It improves linear discriminability of stationary classes, because $\mathbb{E}[|\widehat{X}_y(\omega)|]$ are typically different for different y . However, a linear estimation of $\mathbb{E}[|\widehat{X}_y(\omega)|]$ from a single realization x of X_y has a large variance. It explains the limited performances of a Fourier transform modulus for linear classification.

Fourier modulus descriptors can be improved by using localized filters ψ . If $\sum_u \psi(u) = 0$, then one can verify that $\mathbb{E}[X_y * \psi] = 0$ if X_y is stationary. Theorem 1 shows that the phase of $X_y * \psi$ is again uniformly distributed in $[0, 2\pi]$. It results that $x * \psi$ still provides no linear classification information. This remains true if X_y is only locally stationary (Priestley, 1965) over a domain larger than the support of ψ . This means that its probability distribution is nearly invariant over translations smaller than the support of ψ . A phase collapse then improves linear classification by creating non-zero means $\mathbb{E}[|X_y * \psi|]$. It can improve over Fourier descriptors because the variance of linear estimators of $\mathbb{E}[|X_y * \psi|]$ from a single realization of X_y is reduced when ψ has a small support.

Complex versus real in CNNs: phases and ReLUs The use of complex numbers is a mathematical abstraction which allows introducing a phase variable, and thereby diagonalizing translations. It provides a mathematical interpretation of filtering operations performed on real numbers. We show that a complex network is equivalent to a structured real network.

In the first layer of a CNN, one can observe that filters are usually localized oscillatory patterns (Krizhevsky et al., 2012), where some filters have nearly the same orientations and frequency but have a phase shifted by some α . This means that such filters can be written $\psi_\alpha = \text{Re}(e^{-i\alpha} \psi)$ for a single complex filter ψ and different α . Grouping such channels specifies the complex filter ψ . A CNN with complex filters is thus a structured real-valued CNN, whose channels correspond to phase shifts of these complex filters. This structure simplifies the mathematical interpretation of non-linearities by explicitly defining the phase, which is otherwise a hidden variable relating multiple filter outputs within each layer.

A phase collapse is computed with a modulus. It can be computed by real-valued CNNs by applying ReLUs without biases over filters having different phases: $\psi_\alpha = \text{Re}(e^{-i\alpha}\psi)$. One can verify that:

$$|x * \psi| = \frac{1}{2} \int_0^{2\pi} \text{ReLU}(x * \psi_\alpha) d\alpha. \quad (4)$$

This integral is already well approximated by a sum over 4 phases, allowing to compute complex moduli with ReLUs without biases over real-valued CNN filters.

Thresholding and sparsity versus phase collapse The action of a ReLU can be linearly decomposed into an elimination of sign and a soft-thresholding, which attenuates the amplitude. An important issue is to understand which property is important for classification.

If $z \in \mathbb{R}$ and $b \geq 0$, then the even part of $\text{ReLU}(z - b)$ is $\text{ReLU}(z - b) + \text{ReLU}(-z - b)$, which is an absolute value with a dead-zone $[-b, b]$. It becomes $|z|$ for $b = 0$. The odd part is a soft-thresholding $\rho_b(z) = \text{ReLU}(z - b) - \text{ReLU}(-z - b)$. A soft-thresholding operator over a complex $z = |z| e^{i\varphi}$ reduces the amplitude by b while preserving the phase:

$$\rho_b(z) = \max(|z| - b, 0) e^{i\varphi}. \quad (5)$$

Soft-thresholdings and phase collapses have opposite properties, since soft-thresholdings preserve the phase while attenuating the amplitude, whereas phase collapses preserve the amplitude while eliminating the phase.

If $\mathbb{E}[X_y * \psi] = 0$, then $\mathbb{E}[\rho_b(X_y * \psi)]$ is usually close to 0, because a soft-thresholding is odd. A soft-thresholding thus does not improve much the separability of class means. However, if $\mathbb{E}[X_y * \psi] \neq 0$ and $X_y * \psi$ is sparse, then a soft-thresholding of $X_y * \psi$ may reduce the variance of class mean estimators (Donoho and Johnstone, 1994). It can thus improve linear classification. Coefficients below the threshold may be assimilated to unnecessary “clutter” which is set to 0. To improve classification, convolutional filters must produce high-amplitude coefficients corresponding to discriminative “features”, whereas small-amplitude clutter coefficients are eliminated (Zarka et al., 2021). The dimensionality of sparse representations can also be reduced with random filters which implement a form of compressed sensing (Donoho, 2006; Candes et al., 2006). The interpretation of CNNs as compressed sensing machines with random filters has been studied (Giryet et al., 2015), but it never led to classification results close to the state of the art. On the contrary, we shall see that the use of phase collapse alone reaches this state of the art.

3 PHASE COLLAPSE SCATTERING NETWORK

This section introduces a learned scattering transform, which reaches ResNet accuracy on the ImageNet (Russakovsky et al., 2015) and CIFAR-10 (Krizhevsky, 2009) datasets. It is a highly structured CNN architecture computed with wavelet filters and phase collapse moduli. We describe this architecture and then compare the performance of phase collapse and thresholding non-linearities.

Scattering transform Theorem 1 proves that a phase collapse applied to the output of a complex filter produces a locally invariant descriptor that can then be subsampled, depending upon the filter’s bandwidth. A scattering transform (Mallat, 2012; Bruna and Mallat, 2013) iterates such convolutions with wavelet filters and moduli.

A scattering transform over J scales is implemented with a network of depth J , whose filters are specified by the choice of wavelet. Let $x_0 = x$. For $0 \leq j < J$, a layer x_{j+1} is computed by applying a wavelet filtering operator W and a modulus on x_j :

$$x_{j+1} = |Wx_j|. \quad (6)$$

The operator W is defined with Morlet filters (Bruna and Mallat, 2013). It has one low-pass filter g_0 , and L zero-mean complex band-pass filters g_ℓ , having an angular direction $\ell\pi/L$ for $0 < \ell \leq L$. It thus transforms an input image $x(u)$ into $L + 1$ sub-band images which are subsampled by 2:

$$Wx(u, \ell) = x * g_\ell(2u). \quad (7)$$

Cascading j low-pass filters g_0 with a final band-pass filter g_ℓ , each followed by a subsampling, computes wavelet coefficients at each scale 2^j . One can also modify the wavelet filtering W to compute intermediate scales $2^{j/2}$, as explained in Appendix D. The spatial subsampling is then only implemented every other layer, and the depth of the network becomes twice larger. The number of consecutive moduli can be limited to 2 (Bruna and Mallat, 2013). Applying a linear classifier on such a scattering transform classifier gives good results on simple classification problems such as MNIST (LeCun et al., 2010). However, results are well below ResNet performances on CIFAR-10 and ImageNet, as shown in Table 1.

Phase Collapse Scattering Zarka et al. (2021) showed that a scattering transform can reach ResNet performances by alternating wavelet transform filters with two learned 1×1 convolutional operators. The first is preceded by a ReLU with no bias, and the second is followed by a soft-thresholding non-linearity. Such separable architectures had previously been studied in the context of basis expansion (Qiu et al., 2018; Ulicny et al., 2019) or to filter scattering channels (Cotter and Kingsbury, 2019). However, this learned scattering architecture is difficult to interpret in the context of phase collapses versus thresholdings, because it mixes both. In line with several papers on the use of sparsity for classification (Sun et al., 2018; Sulam et al., 2018; 2019; Mahdizadehghadam et al., 2019; Zarka et al., 2020), Zarka et al. (2021) made the hypothesis that sparsifying neural responses with thresholdings is a major mechanism for improving classification accuracy. The following Phase Collapse Scattering shows that it is in fact not necessary to use any bias nor thresholding. For image classification, it demonstrates that high classification performance mostly results from iterated phase collapses which separate class means.

A Phase Collapse Scattering network applies a complex 1×1 convolutional operator P_j which reduces the channel dimensionality of each x_j , and then applies wavelet filters. The phase of each wavelet coefficient is eliminated by a modulus:

$$x_{j+1} = |WP_j x_j|. \quad (8)$$

Each P_j computes discriminative channels whose spatial variability is eliminated by the phase collapse of complex wavelet coefficients. Table 1 gives the accuracy of a linear classifier applied to the last layer of a Phase Collapse Scattering. It provides an important improvement over a scattering transform, but it does not yet reach the accuracy of ResNet-18.

The final linear classifier is factorized with a 1×1 convolutional operator P_J which reduces the dimension, before linearly combining all channels and positions. The coefficients of x_j are standardized with a zero mean and unit variance along channels before applying the 1×1 convolution P_j . The number of channels of $P_j x_j$ is the same as in a standard ResNet architecture (He et al., 2016) and remains below 512. The norm across channels of $P_j x_j$ for each fixed spatial position is normalized to 1 before applying the wavelet transform W . The architecture uses a total number of layers $J = 11$ for ImageNet and $J = 8$ for CIFAR, by introducing intermediate scales $2^{j/2}$. Details of this Phase Collapse Scattering architecture are provided in Appendix D.

Skip-connections across moduli The architecture of eq. (8) imposes that all phases are collapsed at each layer, after computing a wavelet transform. More flexibility is provided by adding a skip-connection which concatenates $WP_j x_j$ with its modulus:

$$x_{j+1} = \left[|WP_j x_j|, WP_j x_j \right]. \quad (9)$$

The skip-connection produces a cascade of linear filters W without modulus. The resulting linear decomposition $WW \cdots W$ is a “wavelet packet” transform which generalizes the wavelet transform (Coifman and Wickerhauser, 1992; Mallat, 2008). Wavelet packets are obtained as the cascade of low-pass and band-pass filters $(g_l)_l$, each followed by a subsampling. Besides wavelets, wavelet packets include filters having a larger spatial support than wavelets and a narrower Fourier transform. A wavelet packet transform is then similar to a local Fourier transform. Applying a modulus on such wavelet packet coefficients defines local spatial invariants over wider domains.

Image classes are usually not globally invariant to translations. For instance, subjects are generally centered, and some background elements, e.g. the sky, remain at the same spatial position. However, the classes are often locally invariant to translation, up to an unknown maximum scale. Section 2

Table 1: Error of linear classifiers applied to several scattering representations, on CIFAR-10 and ImageNet. The last column gives the single-crop error of ResNet-20 for CIFAR-10 and ResNet-18 for ImageNet, taken from <https://pytorch.org/vision/stable/models.html>.

		Scat	PCScat	PCScat + skip	ResNet
CIFAR-10	Top-1 error (%)	27.7	11.7	7.7	8.8
ImageNet	Top-5 error (%)	54.1	15.2	11.0	10.9
	Top-1 error (%)	73.0	35.9	30.1	30.2

Table 2: Top-1 error (in %) on CIFAR-10 with a linear classifier applied to: a Scattering network (Scat), with Phase Collapse (PCScat), with Amplitude Thresholding (ATScat), with Amplitude Sigmoid (ASScat), and with Amplitude Collapse (ACScat), with or without skip-connections.

	Scat	PCScat	ATScat	ASScat	ACScat
Without skip	27.7	11.7	36.7	51.8	56.2
With skip	-	7.7	22.5	28.7	34.1

explains that a phase collapse improves discriminability for image classes that are locally translation-invariant over the filter’s support. Indeed, their phases are then uniformly distributed over $[0, 2\pi]$, which yields zero-mean coefficients. At a scale where there is no local translation-invariance, these phases are no longer uniformly distributed, and they encode information about the spatial localization of features. Introducing a skip-connection provides the flexibility to choose whether to eliminate phases at different scales or to propagate them up to the last layer, which adds some localization information. This localization information appears to be important for classification.

Table 1 shows that the skip-connection improves classification accuracy. Applying a linear classifier on this Phase Collapse Scattering reaches ResNet-18 accuracy on CIFAR-10 and ImageNet. It demonstrates that collapsing appropriate phases is sufficient to obtain state-of-the-art accuracy, for a given depth, on large-scale classification problems. Learning is reduced to 1×1 filters P_j across channels.

Phase collapse versus amplitude reduction A Phase Collapse Scattering preserves the amplitudes of wavelet coefficients and eliminates their phases. Section 2 explains that it improves separation of class means. On the opposite, one may use a non-linearity which preserves the phases of wavelet coefficients but attenuates their amplitudes. Among such non-linearities is the soft-thresholding, which can improve classification by reducing the variance of class mean estimators, within a sparse representation. The use of sparse representations is usually considered important for image classification (Sun et al., 2018; Sulam et al., 2018; 2019; Mahdizadehghadam et al., 2019). The following results show that it is not the case for images. Several amplitude reduction non-linearities are used, including soft-thresholdings, sigmoids, and an amplitude collapse. We show that it considerably degrades the accuracy compared to a phase collapse, to the point that the classification error becomes larger than with a scattering without learning.

An Amplitude Reduction Scattering applies a non-linearity $\rho(z)$ on each wavelet coefficient $z = |z|e^{i\varphi}$ and preserves the phase: $\rho(z) = e^{i\varphi} \rho(|z|)$. Without skip-connections, each layer x_{j+1} is computed from x_j by:

$$x_{j+1} = \rho(WP_j x_j), \quad (10)$$

and with skip-connections:

$$x_{j+1} = \left[\rho(WP_j x_j), WP_j x_j \right]. \quad (11)$$

A soft-thresholding is defined by $\rho(|z|) = \text{ReLU}(|z| - b)$ for some threshold b . For an amplitude sigmoid we have $\rho(|z|) = (1 + e^{-a|z|-b})^{-1}$, and an amplitude collapse is $\rho(|z|) = 1$. The soft-thresholding and sigmoid parameters a and b are learned for each layer and each channel during the optimization of P_j .

The classification performance of an Amplitude Reduction Scattering is evaluated on CIFAR-10, by applying a linear classifier on the last layer. Classification results are given in Table 2 for different amplitude reductions, with or without skip-connections. Amplitude Reduction Scatterings yield much larger errors than Phase Collapse Scatterings, and these errors are even above a scattering transform without learned 1×1 convolutional projections P_j . It demonstrates that high accuracies result from phase collapses without bias, as opposed to amplitude reduction operators including thresholdings, which learn bias parameters.

ReLU with biases Most CNNs, including ResNet, use ReLUs with biases. As explained in Section 2, a ReLU with bias simultaneously affects the sign and the amplitude of a real coefficient. When decomposing it into its even and odd part, we separate the effects on sign and on amplitude. Over complex numbers, it amounts to transforming the phase or the amplitude. These numerical experiments show that accuracy improvements result from phase collapse as opposed to amplitude reductions, which is a surprising new result.

Several CNN architectures have demonstrated a good classification accuracy with iterated thresholding algorithms, which increase sparsity. However, all these architecture also modified the sign of coefficients by computing *non-negative* sparse-codes (Sun et al., 2018; Sulam et al., 2018; Mahdizadehghadam et al., 2019) or with additional ReLU or modulus layers (Zarka et al., 2020; 2021). It seems that it is the sign or phase collapse of these non-linearities which is responsible for good classification accuracies, as opposed to the calculation of sparse codes through iterated amplitude reductions.

4 ITERATING PHASE COLLAPSES AND AMPLITUDE REDUCTIONS

We now provide a theoretical justification to the above numerical results in simplified mathematical frameworks. This section studies the behavior of phase collapses and amplitude reductions when they are iterated over several layers. It shows that there is no significant gain in performance when iterating amplitude reductions, whereas phase collapses benefit from iterations over multiple layers.

4.1 ITERATED PHASE COLLAPSE

We explain the importance of phase collapses to improve linear classification, as well as the role of iterated phase collapses with multiple filters at each layer, together with learned projectors P_j . For this purpose, we consider the classification of ergodic stationary processes X_y corresponding to different image textures indexed by y . Given a realization x of X_y , and because of ergodicity, the optimal linear classifier is calculated from the empirical mean $1/d \sum_u x(u)$. It computes an optimal linear estimation of $\mathbb{E}[X_y(u)] = \mu_y$. If all textures have the same mean $\mu_y = \mu$, then all linear estimators fail. More precisely, the textures can be linearly separated only if the distance between different means $\|\mu_y - \mu_{y'}\|^2$ is greater than the average estimation error of the empirical means.

If X_y is stationary, then $|X_y * \psi_k|$ remains stationary for any ψ_k . If $\sum_u \psi_k(u) = 0$, then $\mathbb{E}[X_y * \psi_k] = 0$ but $\mathbb{E}[|X_y * \psi_k|] \neq 0$. An optimal linear classifier applied to $|x * \psi_k(u)|$ is obtained by a linear combination of all empirical means $1/d \sum_u |x * \psi_k(u)|$. They are proportional to the ℓ^1 norm $\|x * \psi_k\|_1$, which is a measure of sparsity of $x * \psi_k$.

If linear classification on $|x * \psi_k(u)|$ fails, it reveals that the means $\mathbb{E}[|X_y * \psi_k(u)|] = \mu_{y,k}$ are not sufficiently different for different classes y . These differences can be improved by considering the statistical variations of $|X_y * \psi_k(u)|$ for different y . These variations can be revealed by a new set of filters $\psi_{k'}$ having a zero mean, such as a new set of wavelet filters. Since $\mathbb{E}[|X_y * \psi_k| * \psi_{k'}] = 0$, we must again cancel the phase and compute $\mathbb{E}[|X_y * \psi_k| * \psi_{k'}]$. This phase collapse iteration is the principle used by scattering transforms to discriminate textures (Bruna and Mallat, 2013; Sifre and Mallat, 2013). However, this may still not be sufficiently accurate. More discriminant statistical properties may be obtained by linearly combining $|X_y * \psi_k|$ across k before applying a new filter $\psi_{k'}$.

In a learned Phase Collapse Scattering, the $x * \psi_k$ are combined with a linear projector P_1 across the channel indices k , before computing a convolution with the next filter $\psi_{k'}$. The 1×1 filter P_1 is optimized to improve the linear classification accuracy. It amounts to computing weights w_k

such that $\mathbb{E}[\sum_k w_k |X_y * \psi_k| * \psi_{k'}]$ is as different as possible for different y . It means that the images $\sum_k w_k |x * \psi_k| * \psi_{k'}$ have different sparsity levels depending upon the class y of x . The filter weights of P_1 can thus be interpreted as features along channels providing different sparsifications for different classes. A Phase Collapse Scattering computes such P_j at each scale j .

4.2 ITERATED AMPLITUDE REDUCTIONS

Sparse representations and amplitude reduction algorithms may improve linear classification by reducing the variance of class mean estimations, which can be interpreted as a clutter removal. Such approaches are studied in Zarka et al. (2021) by modeling the clutter as an additive white noise. Although a thresholding algorithm may improve linear classification, we show that iterating filterings and thresholdings does not improve the classification accuracy, if no phase cancellations are inserted.

To understand these properties, we consider the discrimination of classes represented by non-stationary random processes $X_y(u)$. We suppose that they are linearly separable and hence that all $\mathbb{E}(X_y) = \mu_y$ are different for different y . If there exists y' such that $\|\mu_y - \mu_{y'}\|$ is small, then the class y can still be discriminated if we can estimate $\mathbb{E}(X_y)$ sufficiently accurately from a single realization x of X_y . This is a mean estimation problem. Suppose that $X_y = \mu_y + \mathcal{N}(0, \sigma^2)$ is a Gaussian white noise of mean μ_y , where the noise models some clutter. Suppose also that there exists a linear orthogonal operator D such that $D\mu_y$ is sparse, and hence has its energy concentrated in few non-zero coefficients. Such a D may be computed by minimizing the expected ℓ^1 norm $\sum_y \mathbb{E}[\|DX_y\|_1]$. The estimation of μ_y can be improved with a soft-thresholding estimator (Donoho and Johnstone, 1994), which sets to zero all coefficients below a threshold b proportional to σ . It amounts to computing $\rho_b(Dx)$, with $\rho_b(x) = \text{ReLU}(x - b) - \text{ReLU}(-x - b)$.

However, we explain why this approach cannot be further iterated without inserting phase collapses. The reason is that sparsity and entropy of phases are linked, in the sense that a sparse representation concentrates its entropy in the phases of the coefficients, rather than their amplitude. Reciprocally, if the entropy is concentrated in the phases, then the process cannot be further sparsified. The entropy of the phases then needs to be reduced before the next sparsification. This entails that a model of intra-class variability relying on sparsity and amplitude reduction cannot be the sole mechanism behind the performance of deep networks. Iterating sparsity may however be useful if it is alternated with another non-linearity which partly or fully collapses phases. As mentioned in Section 3, this is the case for previous work which used iterated sparsification operators (Sun et al., 2018; Sulam et al., 2018; Mahdizadehghadam et al., 2019). Indeed, these networks compute non-negative sparse codes where sparsity is enforced with a ReLU, which acts both on phases and amplitudes. Our results shows that the benefit of iterating non-negative sparse coding comes from the sign collapse due to the non-negativity constraint.

We now qualitatively demonstrate the two directions of this link with two theorems.

First, we show that finding the sparsest representation of a random process (i.e., minimizing its ℓ^1 norm) is the same as maximizing a lower bound on the entropy of its phases.

Theorem 2. *Let X denote a random vector in \mathbb{C}^d with a probability density p . Let $H(X)$ be the entropy of X with respect to the Lebesgue measure:*

$$H(X) = - \int p(x) \log p(x) dx.$$

Let $D \in U(d)$ be a unitary operator. Then we have:

$$H(\varphi(DX) \mid |DX|) \geq H(X) - d - 2d \log\left(\frac{1}{d} \mathbb{E}[\|DX\|_1]\right).$$

The proof is in Appendix B. This theorem lower-bounds the conditional entropy of the phases of DX by a function of the expected ℓ^1 norm of DX . Minimizing over D this expected ℓ^1 norm amounts to maximizing the lower bound on $H(\varphi(DX) \mid |DX|)$. The extreme situation arises when this entropy reaches its maximal value of $d \log(2\pi)$. $\varphi(DX)$ has then the maximum-entropy distribution, which is the uniform distribution on $[0, 2\pi]^d$. $\varphi(DX)$ is furthermore independent from $|DX|$ in this

extreme case, since its conditional distribution does not depend on $|DX|$. This statistical property has previously been observed on wavelet coefficients of natural images (Rao et al., 2001), as the wavelet transform is an optimal unitary dictionary for sparsity.

Second, we place ourselves in the above extreme case of a random process whose phases are conditionally independent and uniform, and show that it cannot be significantly sparsified in any change of basis.

Theorem 3. *Let X be a random vector of \mathbb{C}^d such that $\varphi(X)$ is uniformly distributed on $[0, 2\pi]^d$ and independent from $|X|$. Then there exists a constant $C_d > 0$ which depends on the dimension d , such that for any $D \in U(d)$,*

$$\mathbb{E}[\|DX\|_1] \geq C_d \mathbb{E}[\|X\|_1].$$

The proof is in Appendix C. This theorem shows that random processes with conditionally independent and uniform phases have an ℓ^1 norm which cannot be significantly decreased by any unitary transformation. Numerical evaluations suggest that the constant C_d may be chosen to be $\sqrt{\pi}/2 \approx 0.886$ independently of the dimension d . This constant is close to one and arises as the ratio between the expected amplitude and standard deviation of a complex normal distribution.

These two theorems explain qualitatively that linear classification on $\rho_b(Dx)$ cannot be improved by another thresholding that would take advantage of another sparsification operator. Indeed, Theorem 2 shows that if Dx is sparse, then its phases have random fluctuations of high entropy. Theorem 3 indicates that such random phases prevent a further sparsification of $\rho_b(Dx)$ with some linear operator. Applying a second thresholding thus cannot significantly reduce the variance of class mean estimators.

5 CONCLUSION

This paper shows that the improvement of linear separability for image classification in deep convolutional networks mostly relies on a phase collapse phenomenon. Eliminating the phase of zero-mean filters improves the separation of class means. We introduced a Phase Collapse Scattering network with wavelet filters and learned 1×1 convolutional filters P_j , which reaches ResNet accuracy. The learned filters P_j enhance discriminability by computing channels that have different levels of sparsity for different classes.

When class means are different, thresholding non-linearities can improve classification by reducing the variance of class mean estimators. However, numerical experiments show that they have a negligible impact on classification accuracy. The iteration of thresholdings on sparsification operators requires intermediary phase collapses. When used alone, the classification performance is poor over complex datasets such as ImageNet or CIFAR-10, because class means are not sufficiently separated.

Our results show that phase collapse are both necessary and sufficient to eliminate spatial variables while linearly separating classes on complex image datasets.

ACKNOWLEDGMENTS

This work was supported by grants from the PRAIRIE 3IA Institute of the French ANR-19-P3IA-0001 program. We would like to thank the Scientific Computing Core at the Flatiron Institute for the use of their computing resources. We also thank Brice Ménard for helpful comments on a previous version of this manuscript.

REFERENCES

- E. Oyallon. *Analyzing and Introducing Structures in Deep Convolutional Neural Networks*. Theses, Paris Sciences et Lettres, October 2017.
- V. Pappayan, X. Y. Han, and D. L. Donoho. Prevalence of neural collapse during the terminal phase of deep learning training. *Proceedings of the National Academy of Sciences*, 2020.
- X. Sun, N. M. Nasrabadi, and T. D. Tran. Supervised deep sparse coding networks. In *2018 25th IEEE International Conference on Image Processing (ICIP)*, pages 346–350, 2018.

-
- J. Sulam, V. Pappas, Y. Romano, and M. Elad. Multilayer convolutional sparse modeling: Pursuit and dictionary learning. *IEEE Transactions on Signal Processing*, 66(15):4090–4104, 2018.
- J. Sulam, A. Aberdam, A. Beck, and M. Elad. On multi-layer basis pursuit, efficient algorithms and convolutional neural networks. *IEEE Transactions on Pattern Analysis and Machine Intelligence*, 2019.
- S. Mahdizadehghadam, A. Panahi, H. Krim, and L. Dai. Deep dictionary learning: A parametric network approach. *IEEE Transactions on Image Processing*, 28(10):4790–4802, Oct 2019.
- J. Zarka, L. Thiry, T. Angles, and S. Mallat. Deep network classification by scattering and homotopy dictionary learning. In *International Conference on Learning Representations, ICLR*, 2020.
- J. Zarka, F. Guth, and S. Mallat. Separation and concentration in deep networks. In *International Conference on Learning Representations, ICLR*, 2021.
- T. Hastie, R. Tibshirani, and J. Friedman. *The elements of statistical learning: data mining, inference and prediction*. Springer, 2 edition, 2009.
- M. B. Priestley. Evolutionary spectra and non-stationary processes. *Journal of the Royal Statistical Society: Series B (Methodological)*, 27(2):204–229, 1965. doi: <https://doi.org/10.1111/j.2517-6161.1965.tb01488.x>. URL <https://rss.onlinelibrary.wiley.com/doi/abs/10.1111/j.2517-6161.1965.tb01488.x>.
- A. Krizhevsky, I. Sutskever, and G. E. Hinton. Imagenet classification with deep convolutional neural networks. In *Advances in Neural Information Processing Systems 25, NeurIPS*, pages 1097–1105, 2012.
- D. L. Donoho and I. M. Johnstone. Ideal spatial adaptation by wavelet shrinkage. *Biometrika*, 81(3): 425–455, 09 1994.
- D. L. Donoho. Compressed sensing. *IEEE Transactions on information theory*, 52(4):1289–1306, 2006.
- E. J. Candes, J. K. Romberg, and T. Tao. Stable signal recovery from incomplete and inaccurate measurements. *Communications on Pure and Applied Mathematics: A Journal Issued by the Courant Institute of Mathematical Sciences*, 59(8):1207–1223, 2006.
- R. Giryes, G. Sapiro, and A. M. Bronstein. Deep neural networks with random gaussian weights: A universal classification strategy? *CoRR*, abs/1504.08291, 2015. URL <http://arxiv.org/abs/1504.08291>.
- O. Russakovsky, J. Deng, H. Su, J. Krause, S. Satheesh, S. Ma, Z. Huang, A. Karpathy, A. Khosla, M. Bernstein, A. C. Berg, and L. Fei-Fei. ImageNet Large Scale Visual Recognition Challenge. *International Journal of Computer Vision (IJCV)*, 115(3):211–252, 2015.
- A. Krizhevsky. Learning multiple layers of features from tiny images. Technical report, 2009.
- S. Mallat. Group invariant scattering. *Communications on Pure and Applied Mathematics*, 65(10): 1331–1398, 2012.
- J. Bruna and S. Mallat. Invariant scattering convolution networks. *IEEE Trans. Pattern Anal. Mach. Intell.*, 35(8):1872–1886, 2013.
- Y. LeCun, C. Cortes, and C.J. Burges. Mnist handwritten digit database. *ATT Labs [Online]*. Available: <http://yann.lecun.com/exdb/mnist>, 2, 2010.
- Q. Qiu, X. Cheng, R. Calderbank, and G. Sapiro. DCFNet: Deep neural network with decomposed convolutional filters. *International Conference on Machine Learning*, 2018.
- M. Ulicny, V. Krylov, and R. Dahyot. Harmonic networks for image classification. In *Proceedings of the British Machine Vision Conference*, Sep. 2019.
- F. Cotter and N. G. Kingsbury. A learnable scatternet: Locally invariant convolutional layers. In *2019 IEEE International Conference on Image Processing, ICIP*, pages 350–354. IEEE, 2019.

-
- K. He, X. Zhang, S. Ren, and J. Sun. Deep residual learning for image recognition. In *2016 IEEE Conference on Computer Vision and Pattern Recognition (CVPR)*, pages 770–778, 2016.
- R.R. Coifman and M.V. Wickerhauser. Entropy-based algorithms for best basis selection. *IEEE Transactions on Information Theory*, 38(2):713–718, 1992. doi: 10.1109/18.119732.
- S. Mallat. *A Wavelet Tour of Signal Processing, Third Edition: The Sparse Way*. Academic Press, 3rd edition, 2008.
- L. Sifre and S. Mallat. Rotation, scaling and deformation invariant scattering for texture discrimination. In *Proceedings of the IEEE conference on computer vision and pattern recognition*, pages 1233–1240, 2013.
- R. Rao, B. Olshausen, M. Lewicki, M. Wainwright, O. Schwartz, and E. P. Simoncelli. Natural image statistics and divisive normalization: Modeling nonlinearities and adaptation in cortical neurons. *Statistical Theories of the Brain*, 01 2001.
- S. Ioffe and C. Szegedy. Batch normalization: Accelerating deep network training by reducing internal covariate shift. In *Proceedings of the 32nd International Conference on International Conference on Machine Learning - Volume 37*, page 448–456, 2015.
- M. Andreux, T. Angles, G. Exarchakis, R. Leonarduzzi, G. Rochette, L. Thiry, J. Zarka, S. Mallat, J. Andén, E. Belilovsky, J. Bruna, V. Lostanlen, M. J. Hirn, E. Oyallon, S. Zhang, C. E. Cella, and M. Eickenberg. Kymatio: Scattering transforms in python. *Journal of Machine Learning Research*, 21(60):1–6, 2020.

A PROOF OF THEOREM 1

We have:

$$\begin{aligned} \|x_\tau * \psi - e^{-i\xi \cdot \tau}(x * \psi)\|_\infty &= \|x * (\psi_\tau - e^{-i\xi \cdot \tau}\psi)\|_\infty && \text{by covariance of convolution,} \\ &\leq \|\psi_\tau - e^{-i\xi \cdot \tau}\psi\|_2 \|x\|_2 && \text{by Young's inequality,} \end{aligned}$$

and then:

$$\begin{aligned} \|\psi_\tau - e^{-i\xi \cdot \tau}\psi\|_2^2 &= \frac{1}{(2\pi)^2} \int_{[-\pi, \pi]^2} |\widehat{\psi}_\tau(\omega) - e^{-i\xi \cdot \tau}\widehat{\psi}(\omega)|^2 d\omega && \text{by Plancherel,} \\ &= \frac{1}{(2\pi)^2} \int_{[-\pi, \pi]^2} |e^{-i\omega \cdot \tau}\widehat{\psi}(\omega) - e^{-i\xi \cdot \tau}\widehat{\psi}(\omega)|^2 d\omega && \text{since } \psi_\tau(u) = \psi(u - \tau), \\ &= \frac{1}{(2\pi)^2} \int_{[-\pi, \pi]^2} |e^{-i\omega \cdot \tau} - e^{-i\xi \cdot \tau}|^2 |\widehat{\psi}(\omega)|^2 d\omega \\ &\leq \frac{1}{(2\pi)^2} \int_{[-\pi, \pi]^2} |(\omega - \xi) \cdot \tau|^2 |\widehat{\psi}(\omega)|^2 d\omega && \text{since } x \in \mathbb{R} \mapsto e^{ix} \text{ is 1-Lipschitz,} \\ &\leq \frac{1}{(2\pi)^2} \int_{[-\pi, \pi]^2} |\omega - \xi|^2 |\tau|^2 |\widehat{\psi}(\omega)|^2 d\omega && \text{by Cauchy-Schwarz,} \\ &= \sigma^2 |\tau|^2, \end{aligned}$$

which leads to the desired result of eq. (3):

$$\|x_\tau * \psi - e^{-i\xi \cdot \tau}(x * \psi)\|_\infty \leq \sigma |\tau| \|x\|_2.$$

B PROOF OF THEOREM 2

We first use the chain rule for the entropy:

$$H(\varphi(DX) \mid |DX|) = H(|DX|, \varphi(DX)) - H(|DX|).$$

The first term is rewritten with a change of variable:

$$\begin{aligned} H(|DX|, \varphi(DX)) &= H(DX) - \sum_{k=1}^d \mathbb{E}[\log |(DX)_k|] \\ &= H(X) - \sum_{k=1}^d \mathbb{E}[\log |(DX)_k|] && \text{as } D \text{ is unitary and hence } |\det(D)| = 1, \\ &\geq H(X) - d \mathbb{E} \left[\log \left(\frac{1}{d} \|DX\|_1 \right) \right] && \text{by concavity,} \\ &\geq H(X) - d \log \left(\frac{1}{d} \mathbb{E}[\|DX\|_1] \right) && \text{by concavity.} \end{aligned}$$

The second term is bounded using the fact that the exponential distribution $\mathcal{E}(\lambda)$ is the maximum-entropy distribution on \mathbb{R}_+ with mean $\frac{1}{\lambda}$:

$$\begin{aligned} H(|DX|) &\leq \sum_{k=1}^d H(|(DX)_k|) \\ &\leq \sum_{k=1}^d \log(e \mathbb{E}[|(DX)_k|]) \\ &\leq d \log \left(\frac{e}{d} \mathbb{E}[\|DX\|_1] \right) && \text{by concavity.} \end{aligned}$$

Combining both inequalities and rearranging terms yield the stated bound:

$$H(\varphi(DX) \mid |DX|) \geq H(X) - d - 2d \log \left(\frac{1}{d} \mathbb{E}[\|DX\|_1] \right).$$

C PROOF OF THEOREM 3

We begin with the following lemma:

Lemma 1. *Let $(\theta_1, \dots, \theta_d)$ be i.i.d. uniform random variables in $[0, 2\pi]$. Then there exists a constant $C_d > 0$ such that for all $(\rho_1, \dots, \rho_d) \in \mathbb{R}^d$, then:*

$$\mathbb{E} \left[\left| \sum_{k=1}^d \rho_k e^{i\theta_k} \right| \right] \geq C_d \sqrt{\sum_{k=1}^d \rho_k^2}.$$

This is proved by noticing that the left-hand side is a norm on \mathbb{R}^d . One can indeed verify that it is positive definite, homogeneous and satisfies the triangle inequality. Since all norms on \mathbb{R}^d are equivalent, there exists a constant $C_d > 0$ such that:

$$\mathbb{E} \left[\left| \sum_{k=1}^d \rho_k e^{i\theta_k} \right| \right] \geq C_d \sqrt{\sum_{k=1}^d \rho_k^2}.$$

for all $(\rho_1, \dots, \rho_d) \in \mathbb{R}^d$.

Going back to the proof of Theorem 3, we then have:

$$\begin{aligned} \mathbb{E} \left[\|DX\|_1 \mid |X| \right] &= \sum_{m=1}^d \mathbb{E} \left[\left| \sum_{k=1}^d D_{m,k} X_k \right| \mid |X| \right] \\ &\geq C_d \sum_{m=1}^d \sqrt{\sum_{k=1}^d |D_{m,k}|^2 |X_k|^2} \quad \text{by the above lemma,} \\ &\geq C_d \sum_{m=1}^d \sum_{k=1}^d |D_{m,k}|^2 |X_k| \quad \text{by concavity, because } \sum_{k=1}^d |D_{m,k}|^2 = 1, \\ &= C_d \|X\|_1 \quad \text{because } \sum_{m=1}^d |D_{m,k}|^2 = 1. \end{aligned}$$

Taking the expectation finishes the proof:

$$\mathbb{E}[\|DX\|_1] \geq C_d \mathbb{E}[\|X\|_1]. \quad (12)$$

D EXPERIMENTAL DETAILS

Channel operators In all experiments we set $P_0 = \text{Id}$, and factorize the classifier with an additional complex 1×1 operator P_J . The architectures implemented are thus also written as $\prod_{j=1}^J P_j \rho W$, where ρ is the non-linearity. Each operator $(P_j)_{1 \leq j \leq J}$ is preceded by a standardization. It sets the complex mean $\mu = \mathbb{E}[z]$ of every channel to zero, and the real variance $\sigma^2 = \mathbb{E}[|z|^2]$ of every channel to one. This is similar to a complex 2D batch-normalization layer (Ioffe and Szegedy, 2015), but without learned affine parameters. Each operator $(P_j)_{1 \leq j \leq J}$ is additionally followed by a spatial divisive normalization (Rao et al., 2001), similarly to the local response normalization of Krizhevsky et al. (2012). It sets the norm across channels of each spatial position to one. The sizes of the $(P_j)_j$ are specified in Table 3. The total numbers of parameters for each architecture are specified in Table 4.

Spatial filters We use elongated Morlet filters for the L complex band-pass filters $(g_\ell)_l$ which are rotated versions of a mother wavelet g : $g_\ell(u) = g(r_{-\pi\ell/L}u)$, with r_θ the rotation by angle θ . The mother wavelet g is defined as:

$$g(u) = \frac{\sigma^2}{2\pi/s^2} (e^{i\xi \cdot u} - K) e^{-u \cdot \Sigma u / 2} \quad \text{with } \Sigma = \begin{pmatrix} \sigma^2 & 0 \\ 0 & \sigma^2 s^2 \end{pmatrix}, \quad (13)$$

Table 3: Number c_j of complex output channels of P_j , $1 \leq j \leq J$. The total number of layers is $J = 8$ for CIFAR and $J = 11$ for ImageNet.

	j	1	2	3	4	5	6	7	8	9	10	11
CIFAR-10	c_j	64	128	256	512	512	512	512	512	-	-	-
ImageNet	c_j	32	64	64	128	256	512	512	512	512	512	256

Table 4: Number of real parameters (in millions) of Phase Collapse Scattering network architectures. A complex parameter is counted as two real parameters.

	PCScat	PCScat + skip	ResNet
CIFAR-10	41.6	83.1	0.27
ImageNet	36.0	62.8	11.7

Its center frequency is $\xi = ((3\pi/4)/2^\gamma, 0)$, its bandwidth $\sigma = 1.25 \times 2^{-\gamma}$, and its slant $s = 0.5$, where 2^γ designates the scale of the band-pass filter.

g is rotated along $L = 8$ angles for Imagenet and $L = 4$ angles for CIFAR: $\theta_\ell = (\pi\ell/L)_{1 \leq \ell \leq L}$. The g_ℓ are then discretized for numerical computations, and K is adjusted so that they have a zero mean.

Finally, we use for the low frequency g_0 a Gaussian window:

$$g_0(u) = \frac{\sigma^2}{2\pi} e^{-\sigma^2 \|u\|_2^2 / 2}.$$

The filters are implemented with the *Kymatio* package (Andreux et al., 2020).

Intermediate scales $2^{j/2}$ are obtained by applying a subsampling by 2 after each block of 2 layers. This introduces intermediate scales and generates a wavelet filterbank with 2 scales per octave: the filters are designed so that when j low-pass filters and one band-pass filter are cascaded, with a subsampling every 2 layers, the scale of the resulting wavelet is $2^{j/2}$.

Each block comprises in its first layer a low-frequency filter g_0^1 with $\gamma = -1/2$ and band-pass filters with $\gamma = 0$. In the second layer, we use the same low-frequency filter $g_0^2 = g_0^1$ with $\gamma = -1/2$. The band-pass filters g_ℓ^2 are obtained with parameters $\xi' = (\pi/\sqrt{2}, 0)$, $\sigma' = 1.25\sqrt{2/3}$, and $s' = \sqrt{0.2}$.

For CIFAR experiments, the $J = 8$ layers are grouped in 4 successive blocks of 2 layers. For ImageNet experiments, the first layer consists of band-pass elongated Morlet filters g_ℓ and a low-pass gaussian window g_0 with $\gamma = 0$, followed by a subsampling of 2. The 10 following layers are grouped in 5 successive blocks of 2 layers.

Optimization We use the optimizer SGD with an initial learning rate of 0.01, a momentum of 0.9, a weight decay of 0.0001, and a batch size of 128. The classifier is preceded by a 2D batch-normalization layer. We use standard data augmentation: horizontal flips and random crops for CIFAR, random resized crops of size 224 and horizontal flips for ImageNet. Classification error on ImageNet validation set is computed on a single center crop of size 224. On CIFAR, training lasts for 300 epochs and the learning rate is divided by 10 every 70 epochs. On ImageNet, training lasts for 150 epochs and the learning rate is divided by 10 every 45 epochs. The experiments in the paper required around 10k 32GB NVIDIA V100 GPU-hours.